Available online at www.sciencedirect.com
ScienceDirect
Journal of Molecular Catalysis A: Chemical 275 (2007) 214–227
JOURNAL OF MOLECULAR CATALYSIS A: CHEMICAL
www.elsevier.com/locate/molcata

Proton enriched high-surface-area cesium salt of phosphotungstic heteropolyacid with enhanced catalytic activity fabricated by nanocasting strategy

P. Madhusudhan Rao [a], P. Goldberg-Oppenheimer [a], S. Kababya [b], S. Vega [b], M.V. Landau [a,*]

[a] *Chemical Engineering Department, Blechner Center for Applied Catalysis and Process Development, Ben-Gurion University of the Negev, Beer-Sheva 84105, Israel*
[b] *Department of Chemical Physics, Weizmann Institute of Science, Rehovot 76100, Israel*

Received 22 April 2007; received in revised form 29 May 2007; accepted 30 May 2007
Available online 8 June 2007

Abstract

The elimination by HF of the silica matrix from the composites obtained by the two-step reaction deposition of $Cs_xH_{3-x}PW_{12}O_{40}$ (CsHPW) salt nanocrystals with a Cs/W_{12} ratio equal 2.5 on SBA-15 yields materials with substantially lower Cs/W_{12} ratios of 1.7–2.0. The value of the Cs/W_{12} ratio in the nanocasts is determined by the Cs-precursor (Cs *n*-propoxide or Cs-acetate) used at the first stage of materials preparation. The surface area of the CsHPW nanocasts is 41–45 times higher than their co-precipitated analogs at the same Cs/W_{12} ratios. We report here that implementation of the nanocasting preparation technique yields for the first time a bulk CsHPW material that combines a high concentration of acid sites ($Cs/W_{12} = 1.7$–2.0) with a high surface area of 41–93 $m^2\,g^{-1}$. Co-precipitated analogues at the same Cs/W_{12} ratios are nonporous and exhibit a surface area smaller than 5 $m^2\,g^{-1}$. Our nanocasted CsHPW materials are stable against leaching and colloidization in polar solvents, and their catalytic performance exceeded that of bulk $Cs_{2.5}H_{0.5}PW_{12}O_{40}$, known as the most active among the acidic HPW salts. The catalytic activity of CsHPW nanocasts in MTBE synthesis and in the isopropanol dehydration reactions is shown to be higher by a factor of 2–3 than that of the standard $Cs_{2.5}H_{0.5}PW_{12}O_{40}$ material.

Keywords: Heteropolyacid; Cs salt; SBA-15 silica; Nanocasting; Surface acidity; Acid catalyst

1. Introduction

Dodecatungstophosphoric acid $H_3PW_{12}O_{40}$ (hereafter HPW) is the strongest acid among the heteropolyacids that has been employed as catalysts in reactions of hydrocarbons, such as acylation, alkylation, esterification, isomerization, etc. [1,2]. Its low surface area (<5 $m^2\,g^{-1}$), limiting the accessibility to its acid sites, and its high affinity to polar solvents, making it soluble, called for suitable modification of the bulk acid. The two approaches that have addressed these two characteristics and their consequences are the dispersion and chemical fixation of the acid on an oxide support [3,4] and the conversion of the acid into a corresponding alkali metal salts, yielding an acidic material insoluble even in polar solvents [5]. The loss of acidic protons in the alkali metal salts is compensated by an accompanied increase in microporosity. This has been observed for cesium salts exhibiting a Cs/W_{12} ratio larger than 2 [6,7]. This microporosity increases the accessibility of reacting molecules to acid sites in these Cs-salts as compared to salts with Cs/W_{12} ratios smaller than 2 that are nonporous and have surface area smaller than 3 $m^2\,g^{-1}$ [2,5]. The CsHPW salts with $Cs/W_{12} > 2$ have been widely tested, and it was found that the composition $Cs_{2.5}H_{0.5}PW_{12}O_{40}$ shows the highest catalytic activity [2,8].

The tendency of the cesium salts of HPW (hereafter CsHPW) to form milky suspensions in polar substrates, thus creating filtration problems in liquid phase reactions and a pressure drop in fixed bed reactors, limits their practical applications [9]. This drawback can be circumvented by stabilizing CsHPW in porous oxide matrices [10–19]. Besides fixation of CsHPW, preventing its colloidization in polar solutions, the main research effort in these materials has been to increase the catalytic activity of the

* Corresponding author. Tel.: +972 8 647 2141; fax: +972 8 647 9427.
E-mail address: mlandau@bgu.ac.il (M.V. Landau).

1381-1169/$ – see front matter © 2007 Elsevier B.V. All rights reserved.
doi:10.1016/j.molcata.2007.05.046

salt with the optimal composition by increasing the dispersion of its crystals.

Soled et al. [10] proposed an original solution that was intended to solve two practical difficulties: the insertion of insoluble CsHPW salt inside the pores of silica-gel and the appearance of fine dispersions of Keggin units that partially exchange with Cs^+-ions at the supports surface. They accomplished this by a "reaction deposition" technique consisting of two steps: first grafting of Cs^+-ions onto the silica surface (1) followed by an exchange of these surface Cs^+-ions with protons of the HPW molecules dissolved in water (2). This resulted in a deposition of insoluble Cs-salt inside the pores of the silica.

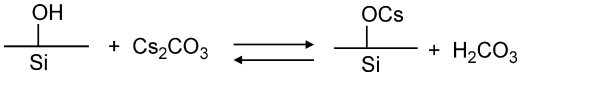

(1)

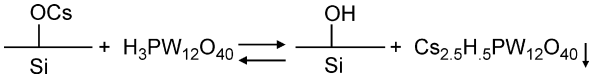

(2)

A problem with this procedure has been the precipitation of CsHPW salt on the outer spheres and at the external surfaces of the silica-gel pellets during step (2). Later Wang et al. [13,14] suggested that the Cs^+ cations that are grafted during step (1) are re-dissolved in the acidic aqueous solution of HPW via hydrolysis of the Si–O–Cs moieties at step (2). This enables the migration of Cs^+ cations to the outer surface of the silica particles, causing a lowering of the dispersion of the supported CsHPW. The improved reaction deposition technique using HPW solutions in non-aqueous solvents, especially in alcohols that does not hydrolyze the O–Cs bonds, yielded a uniform distribution of CsHPW salt in MCM-41 crystals versus segregated CsHPW/MCM-41 and CsHPW phases obtained from aqueous solution, as observed by TEM [13].

Implementation of this improved technique resulted in a series of CsHPW catalytic materials supported on silica-gel [11,12], on mesostructured silicas MCM-41 [12–15] and SBA-15 [16], on amine-modified silica [17] as well as on alumina-silicas K-10 clay [18] and zeolite USY [19] that demonstrated better catalytic performance compared with bulk salt. The deposition of CsHPW on silica using the optimized reaction deposition methods increased its specific activity by 2–10 times, calculated based on the weight of the catalytic phase and depending on the texture of the support, the loading and type of the catalytic reaction. Unfortunately, most of these effects are compensated by a dilution of the catalytic phase with the inert silica. As a result the activity of the supported catalysts does not exceed the activity of their bulk counterparts by more than 50%, when based on the total weight of the catalyst.

The real chemical composition of the CsHPW phase and its accessible surface inside supporting composite materials, determining the potential performance of the catalytic phase, remain unknown. It was shown that all the existing protons in bulk microporous CsHPW with a crystal size of 12 nm and a Cs/W_{12} ratio of 2.5 are available for adsorption of NH_3 [6] and pyridine [20]. This makes it doubtful that a further increase of the acidity and catalytic activity can be expected for decreasing crystal sizes to less than 10 nm. Another source for a possible increase of the catalytic reaction rates by diminishing the diffusion limitations of reagents/products should be ruled out, since the diffusion limitations in microporous materials like zeolites are insignificant in this range of crystal sizes [21].

Absorption measurements have demonstrated a more than 3-fold increase of the amount of adsorbed ammonia per gram of CsHPW phase after its insertion in SBA-15 at a nominal Cs/W_{12} ratio of 2.5 [16]. The 2–10-fold increase of specific catalytic activities after deposition of CsHPW salts on silica observed by several groups is consistent with these data. One of possible explanations for these phenomena could be the formation and fixation of highly acidic nanocrystals of the CsHPW phase with $Cs/W_{12} < 2.5$ inside the silica pores. The high catalytic activity of such proton enriched materials on silica supports, prepared at low nominal Cs/W_{12} ratios, was observed previously [11,12]. The potential performance of these nanocrystals would be even higher if no blockage of part of them inside silica pores would occur.

In the present work we will show that indeed in a material supporting CsHPW and showing a nominal Cs/W_{12} ratio equal to 2.5 the actual Cs/W_{12} ratio of the CsHPW crystals, after the removal of the support, is substantially lower. The reason for this being that part of the Cs ions inserted at step (1) can be located in silica micropores and that during step (2) of the reaction deposition part of the Cs atoms are not accessible for the $Cs^+ \leftrightarrow H^+$ exchange reaction with the bulky Keggin anions, thus yielding a substantially lower actual Cs/W_{12} ratio in supported nanocrystals than following from the nominal composition.

This was confirmed by implementation of nanocasting strategy [22] for preparation of CsHPW materials where they were first stabilized in the mesoporous matrix playing a role of a scaffold for catalytic phase and then liberated from the matrix forming a nanocast. In the next sections the materials at the different stages of the preparation of the CsHPW nanocasts by reaction deposition and matrix extraction using SBA-15 support as a scaffold are characterized with the help of HRTEM, HRSEM, EDX, N_2 adsorption, WAXS, NH_3-TPD, XPS and MAS NMR. In addition the catalytic performance of the resulting nanocasts with Cs/W_{12} ratios smaller than 2 and with high surface area of 41–93 $m^2\,g^{-1}$ are tested via several acid-catalyzed reactions.

2. Experimental

2.1. Preparation of the materials

Bulk CsHPW samples with a Cs/W_{12} ratio between 1.5 and 2.5 were prepared from aqueous solutions of Cs_2CO_3 (Aldrich) and $H_3PW_{12}O_{40}$ (Aldrich) by titration according to a previously reported procedure [5,23]. An appropriate amount of aqueous solution of Cs_2CO_3 (0.2 mol/l) was added dropwise to an aqueous solution of HPW (0.08 mol/l) at a rate of ~1 ml/min. The milky colloidal solution was stirred overnight and then evaporated at 318 K. The remaining solid was finally calcined in air at 573 K for 2 h.

SBA-15 employed in this study was prepared, following the procedure described elsewhere [24], via crystallization from

an acidic aqueous solution of poly(ethylene glycol)-block-poly(propylene glycol)-block poly(ethylene glycol)-copolymer (M_{avg} = 5800) and TMOS. The surfactant mediating the SBA-15 structure was finally removed by burning at 773 K. The CsHPW was inserted in the SBA-15 silica matrix by the two-step reaction deposition method. The parent CsHPW/SBA-P (Cs-precursor Cs-*n*-propoxide) and CsHPW/SBA-A (Cs-precursor Cs-acetate) samples were obtained by dispersing the surfactant free SBA-15 (0.5 g) in 10 ml of *n*-propanol followed by an addition of 0.15 ml of 33% cesium *n*-propoxide in *n*-propanol or an addition of 0.2 g of cesium acetate (Aldrich), respectively. The contents were stirred for 4 h, filtered and evacuated at room temperature, until they were dry. During step (2) of the preparation procedure the dry solids were treated for 12 h with a solution containing an excess of HPW dissolved in *n*-propanol under continuous stirring, after which they were filtered and washed with an excess of *n*-propanol. The resulting solids were dried at 383 K for 2 h and calcined at 573 K for another 2 h. The cesium *n*-propoxide in *n*-propanol was prepared by adding cesium metal (Alfa Aesar, 99% purity) to an excess of *n*-propanol under continuous stirring [25] and stored in a glove box.

The silica matrix was gradually removed from the CsHPW/SBA materials by a treatment with HF. Half a gram of the CsHPW/SBA-P (or -A) composites were continuously stirred in 20 ml of an aqueous HF solution for 3 h at room temperature. The solid was recovered by decantation after centrifugation (7000 rpm). The water addition/centrifugation sequence was repeated three times and finally the material was evacuated at 333 K. The extent of removal of the silica, ranging from 7 to 93%, was controlled by varying the HF concentration in the solution from 0.3 to 10%. The HF treated materials were denominated as CsHPW/SBA-HF-NP or CsHPW/SBA-HF-NA, where *N*—number of HF treatments, P or A indicate the type of Cs-precursor as described above.

2.2. Characterization of the materials

The chemical composition of the bulk CsHPW samples and the CsHPW loading in the SBA-15 supported materials and their nanocasts were estimated by averaging the results of energy dispersive X-ray spectroscopy (EDS) experiments at five different positions in the samples. For these measurements a JEOL JEM 5600 scanning electron microscope link system AN-1000, equipped with a Si–Li detector, was used. The Cs content in CsHPW materials was characterized by the Cs/W_{12} further defined as Cs/W_{12} ratio calculated from the atomic percentages of Cs and W in samples according to EDS data. This ratio was estimated more accurate than the Cs/P ratio due to absence of EDS peaks superposition in the first case. Surface area and pore volumes were derived from N_2 adsorption–desorption isotherms, using the conventional BET and BJH methods. The pore size distributions were calculated from the desorption branch of the N_2-sorption isotherms by using the NLDFT kernel of the Autosorb software package, provided by Quantachrome, and applying as a model the adsorption of nitrogen on silica at 77 K. The samples were degassed under vacuum for 2 h at 373 K. Isotherms were measured using a static-volumetric method at liquid nitrogen temperature with a NOVA-2000 (Quantachrome, Version 7.02) instrument.

Conventional wide-angle XRD (WAXS) and SAXS patterns were obtained with a Philips 1050/70 powder diffractometer (Bragg-Brentano geometry), fitted with a graphite monochromator providing a Kα diffracted beam (λ = 1.541 Å) and operating at V = 40 kV and I = 30 mA, using software developed by Crystal Logic. The data were collected in a range of 2θ values between 3° and 90° with a step size of 0.005°. SAXS patterns were recorded with the narrow X-ray beam. These data were obtained with a 0.02° step size and a data collection of 2 s at each step. X-ray photoelectron (XPS) spectra were acquired with a PHI 549 SAM/AES/XPS ultra-high-vacuum (10^{-9} Torr) apparatus with a double-cylindrical mirror analyzer (CMA) and a Mg Kα (1253.6 eV) X-ray source. Powder samples of the catalysts were pressed on the indium-plated grid to a thin layer.

High resolution SEM (scanning electron microscope) micrographs were obtained on a JEOL JSM 7400 FESEM microscope operated at 3 kV with a working distance of 2.6–8 mm and a resolution of up to 1 nm. The samples were coated with chromium to avoid charging effects and improve the image quality. High resolution TEM (Transmission Electron Microscope) (HRTEM) micrographs of the nanocasted materials were obtained using a JEM 2010 microscope operating at 200 kV and equipped with EDS. The samples for HRTEM were prepared by depositing a drop of an ultrasonicated ethanol suspension of solid catalyst on the carbon coated copper grid. The grid was dried in vacuum and mounted on a specimen holder. The composite CsHPW/SBA-15 samples for HRTEM were embedded in a resin and ultra-microtomed into slices with a thickness of ∼50 nm mounted on a Cu grid. The HRTEM micrographs of as-prepared composite materials were obtained using a Tecnai G^2 instrument operating at 120 kV.

TPD experiments of ammonia were performed in a AMI-100 Catalyst Characterization System (Zeton-Altamira) equipped with a TCD detector and a mass-spectrometer for the identification of the outlet components (Ametek 1000). Approximately 0.4 g of catalyst was loaded in the sample holder and heated to 873 K in argon and subsequently cooled to 298 K. After dosing with a 5 vol% of ammonia in argon mixture at a flow rate of 30 ml min^{-1} for 30 min the system was purged with argon for 1 h at the same temperature. The temperature was increased at a ramp of 10 K min^{-1} to 423 K in argon and was held for 30 min to expel physisorbed ammonia. After cooling to 298 K the temperature was raised to 873 K at a rate of 10 K/min and the outlet gases were analyzed by a thermal conductivity detector and a mass spectrometer.

^{1}H, ^{31}P and ^{133}Cs NMR experiments were carried out on a DSX-300 Bruker spectrometer operating at 300.14, 121.5 and 39.37 MHz, respectively. A BL 4 mm Bruker MAS double resonance probe was used at ambient temperature. The spinning frequency was 10 kHz during the ^{1}H experiments and 5 and 2.5 kHz during the ^{31}P and ^{133}Cs experiments. The proton spectra were measured by using a Hahn-echo sequence with a pulse-spacing of 100 μs and at a repetition time of 5 s. The pulse lengths were 3 and 6 μs. All Fourier transformed spectra were obtained after an accumulation of four transients. The

^{31}P and ^{133}Cs signals were measured after the application of a single excitation pulse and during a proton decoupling of 80 kHz. The pulse lengths and flip angles were 5 μs and 50° for ^{133}Cs- and 5 μs and 90° for ^{31}P-detection and signals were accumulated with a repetition time of 60 and 600 s for ^{31}P and ^{133}Cs, respectively. Four signals were accumulated before Fourier transformation.

Proton decoupled signals were detected after variable amplitude cross-polarization MAS (VACPMAS) or after applying a single 90° excitation pulse. The proton decoupling power was 62 kHz for both types of experiments. The Hartman–Hahn matching conditions were set around 62 kHz and the duration of the matching time was 5 ms. The repetition times were 4 and 600 s and 300 and 2000 signals were accumulated in order to obtain sufficient signal to noise for the VACPMAS and the single pulse experiments, respectively. The ^{31}P chemical shift scale was referenced to H_3PO_4 (85%) and the ^{133}Cs scale to CsCl.

2.3. Testing of the materials

All the CsHPW based catalysts were treated, prior to the tests of their catalytic performance, by a nitrogen flow of 2 h at 473 K. The MTBE synthesis was carried out in the liquid phase as follows: 4.26 g of both methanol (Frutarom) and *t*-butanol (Aldrich) were loaded in a 20 ml stainless steel reactor followed by the addition of 20 mg of freshly activated catalyst. The reaction was carried out at 383 K for 2 h under continuous stirring. The liquid products were analyzed for MTBE by GC using an HP-5890, Series II instrument, fitted with a capillary column HP-1 (100% dimethyl polysiloxane). In a typical isopropanol (IP) dehydration reaction, 16 g of isopropanol (Frutarom) and 60 mg of catalyst were loaded into the reactor and stirred at 473 K for 2 h. The product, di-isopropyl ether (DIPE) and unreacted reagents after separation from the catalyst were analyzed as in the case of the MTBE synthesis.

The catalytic activity was expressed in terms of the intrinsic rate of product formation per weight of loaded catalyst, $r_{cat} = N_i\,\tau^{-1}\,W_{cat.}{}^{-1}$ (mmol h^{-1} g cat^{-1}), or per 1 m^2 of loaded catalyst $r_{cat} = N_i\,\tau^{-1}\,S_{cat.}^{-1}$ (mmol h^{-1} m^{-2}), where N_i is mmol of reaction product (MTBE or DIPE) at the end of the run and τ the run time (h). $W_{cat.}$ is the mass of the catalyst (g) and $S_{cat.}$ (m^2 g^{-1}) the surface area per gram of the catalyst. The operating conditions for each of the two reactions were chosen so that external and internal diffusion limitations were excluded and the conversion of the reagents did not exceed 30%.

3. Results and discussion

3.1. Chemical composition and materials texture

After the removal of the surfactant by calcination in air at 773 K the SBA-15 silica displayed a surface area of 873 m^2/g, a pore volume of 1.4 cm^3/g, an uniform pore size distribution centered at ~7 nm (derived from the desorption branch of the N_2-adsorption isotherm) and a micropore surface area of 88 m^2/g. Its crystals had a cylindrical form with 3–4 μm diameter and 5–15 μm length and consisted of accreted parallel cylindrical fibers 300–500 nm in diameter (from the analysis of SEM micrographs). Each of these fibers, according to HRTEM micrographs, consisted of ~2000 parallel nanotubular pores with walls of a width of 4–5 nm. The small angle XRD pattern of the parent SBA-15 samples included a high intensity peak (1 1 1) with a d-spacing of 10.5 nm and two less intensive reflections with *d*-values consistent with a hexagonal arrangement of the pores with a 11.7 nm distance between their axes, in agreement with the HRTEM data.

The chemical composition and texture characteristics of our parent SBA-15, of the starting CsHPW/SBA-P and CsHPW/SBA-A composites and of the materials obtained after progressive removal of the silica matrix from these composites are shown in Table 1. With both Cs sources it was possible to insert by reaction deposition similar amounts of the CsHPW phase, corresponding to a 42(46) wt.% loading at a nominal Cs/W_{12} ratio of ~2.5. The percentage of silica matrix removed from the CsHPW/SBA composites varied over a wide range from 7 to 93%. At the highest level of desilication a negligible amount of SiO_2 (<5 wt.%) was left in the sample.

3.2. The Cs/W_{12} ratios

The Cs/W_{12} ratios decreased adversely proportional to the extent of desilication of the materials. In the purest CsHPW nanocasts with 4 wt.% SiO_2, CsHPW/SBA-HF-5P and CsHPW/SBA-HF-2A (Table 1), the Cs/W_{12} values were 1.7 and 2.0, respectively—significantly lower than the nominal composition of the CsHPW phase in the parent CsHPW/SBA composites. This result was consistent with XPS measurements of the chemical composition of the surfaces of these CsHPW nanocasts and of a bulk reference $Cs_{2.5}H_{0.5}PW_{12}O_{40}$ sample. Atomic adsorption analysis (Varian AA240FS instrument, wavelength 400.9 nm for W and 894.1 nm for Cs) of the solutions obtained after dissolution the starting CsHPW/SBA-P, CsHPW/SBA-A composites and their nanocasts CsHPW/SBA-HF-5P and CsHPW/SBA-HF-2A (Table 1) in 40% aqueous NaOH yielded the values of Cs/W_{12} ratios being in good agreement with the results obtained by EDX method with deviation in the range of ± 0.05. The composites with lower nominal Cs/W_{12} ratios smaller than 1 were not stable even after calcination as the excess HPW (beyond an equilibrium value corresponding to Cs/W_{12} ratios after silica removal of 1.7 and 2.0, respectively) leached out when contacted with polar solvents resulting in the equilibrium Cs/W_{12} ratio. In our preparation the Cs/W_{12} ratios in the composites were pre-determined by the amount of Cs inserted to SBA-15 at the first step. The Cs/SBA-15 material was treated with excess HPW. There seems to be an equilibrium Cs/W_{12} ratio that is largely determined by the nature of Cs precursor.

The lower Cs/W_{12} ratios in nanocasts relative to their nominal values in starting composites can be a result of two phenomena: (i) fixation of part of the Cs ions at surface silanols inside the micropores of SBA-15 silica crystals, making them non-available for reaction with the bulky heteropolyanions of HPW during step (2) of

Table 1
Chemical composition and texture characteristics of parent CsHPW/SBA-15 and their nanocasts in comparison with the bulk $Cs_{2.5}H_{0.5}PW_{12}O_{40}$ and $H_3PW_{12}O_{40}$ materials

No.	Sample	Chemical composition			SiO_2 removed (%)	Texture parameters (N_2 adsorption)			CsHPW crystal size (nm)	
		SiO_2 (wt.%)	CsHPW (wt.%)	Cs/W_{12}		Surface area (m^2/g)	Pore volume (cm^3/g)	Pore diameter (nm)	XRD	HRTEM
1	SBA-15	100	–	–	–	873	1.4	6.4	–	–
2	CsHPW/SBA-P	58	42	2.5	0	432	0.59	5.5	7.5	5–9
3	CsHPW/SBA-HF-1P	54	46	2.3	7	344	0.48	5.6	–	–
4	CsHPW/SBA-HF-2P	33	67	2.0	43	205	0.33	6.4	–	–
5	CsHPW/SBA-HF-3P	29	71	1.9	50	119	0.19	6.6	–	–
6	CsHPW/SBA-HF-4P	16	84	1.8	74	70	0.10	5.5	–	–
7	CsHPW/SBA-HF-5P	4	96	1.7	93	41	0.05	4.8	7.5	5–9
8	CsHPW/SBA-A	54	46	2.5	0	464	0.64	5.5	7.0	5–8
9	CsHPW/SBA-HF-1A	28	72	2.2	48	164	0.25	6.1	–	–
10	CsHPW/SBA-HF-2A	4	96	2.0	93	93	0.07	3.1	7.0	5–8
11	Bulk $Cs_{2.5}H_{0.5}HPW_{12}O_{40}$	–	100	2.5	–	149	0.11	2.8	13	12–15
12	Bulk $H_3PW_{12}O_{40}$	–	–	0	–	6	0.01	6.4	85	70–100

the reaction deposition or (ii) the occurrence of an ion exchange of the form $Cs_{2.5}H_{0.5}PW_{12}O_{40} + xHF \rightarrow Cs_{2.5-x}H_{0.5+x}PW_{12}O_{40} + xCsF$ during the silica removal step with aqueous HF. The possible fixation (i) of part of the Cs ions inside the micropores of SBA-15 matrix is consistent with the decrease of the micropore surface area derived from N_2-adsorption isotherms by the t-plot method. The micropore surface area decreased from 88 m^2/g to the zero after insertion of cesium, using both Cs-propoxide and acetate precursors. The availability of only part of the Cs's to HPW heteropolyacid inside the mesopores of SBA-15 should cause a formation of nanocrystals of the form Cs_xH_{3-x} $PW_{12}O_{40}$ with $x < 2.5$, *i.e.* lowering of the real Cs/W_{12} ratio in the CsHPW crystals compared to the nominal composition. During the removal of silica the excess amount of cesium located inside the micropores will then pass to the solution being dissolved in aqueous HF together with silica matrix. Cesium was indeed found in the filtrate of this solution by atomic adsorption analysis. This can explain the gradual decrease of the Cs/W_{12} value in the nanocasts with increasing extent of desilication, as shown in Table 1. The fact that the Cs/W_{12} value measured in the CsHPW/SBA-HF-5P nanocast is lower than that in CsHPW/SBA-HF-2A can be a result of a higher affinity of basic Cs-propoxide to acidic silanols than of Cs-acetate, favoring the penetration of Cs into the micropores in the first case.

The second option (ii) – the ion exchange $Cs^+ \leftrightarrow H^+$ during desilication in aqueous HF – can also yield cesium in the filtrate of the aqueous HF solution. The reference co-precipitated $Cs_{2.5}H_{0.5}PW_{12}O_{40}$ salt with the surface area of 149 m^2/g was treated with a 10% aqueous HF solution as was done for removal of silica matrix from the CsHPW/SBA-15 composites. Also the $Cs_{2.5}H_{0.5}PW_{12}O_{40}$ salt was treated with aqueous HF in three parallel experiments. According to EDS analyses the Cs/W_{12} ratios of these solids did not decrease below the value of 2.4, corresponding to the accuracy of the method at an actual Cs content that is larger than 10%. This indicates that any ion exchange in aqueous HF is negligible and cannot explain the reduction of the Cs/W_{12} ratio in nanocasted materials. This conclusion is consistent with the reported ion-exchange characteristics of CsHPW salts. The equilibrium of the ion exchange $H^+ \leftrightarrow Cs^+$ in aqueous solutions of heteropolyacids is strongly shifted to the right due to the high acid strength of HPW ($-H_0 = 13.16$). Thus the acid easily adsorbs Cs-ions [26] and the resulting CsHPW salt cannot be dissolved in an acid that was confirmed by absence of W in HF-solutions after silica extraction. In addition the steric hindrance for removal the bulk Cs^+ ions shifts the equilibrium to the right, as was found for the ion-exchange mechanisms, $K^+ \leftrightarrow Cs^+$ and $NH_4^+ \leftrightarrow Cs^+$, in corresponding salts of HPW acid [27].

3.3. Materials fluorination

The co-precipitated $Cs_{2.5}H_{0.5}PW_{12}O_{40}$ salt treated with HF, as well as the nanocasted CsHPW/SBA-HF-5P and CSHPW/SBA-HF-2A materials were analyzed also for fluorine content. The possible fluorination of the CsHPW nanocasts can affect their acidity and catalytic performance. The fluorine analysis was done by two methods: EDX (sensitivity > 0.5 wt.%) and potentiometric titration with an ion-selective electrode (ICE type for F^-, No. 6.0502.150, Metrohm Co.) after dissolution of the samples in 40% aqueous NaOH (sensitivity >0.05 wt.%). Both methods did not detect any fluorine in the tested samples. This abandons the possibility of a significant modification of the acidic properties of nanocasted CsHPW materials due to their fluorination at the desilication step.

3.4. Electron microscopy

In the as-prepared CsHPW/SBA-15 composites all the CsHPW material was located inside the pores of SBA-15 silica crystals. SEM did not reveal any CsHPW particles at the external surface or between the microfibers, building the crystals of mesostructured silica (Fig. 1a). However, isolated 5–9 nm nanoparticles of CsHPW were clearly observed by HRTEM in the curved nanotubular channels inside the silica microfibers (Fig. 2). Part of the CsHPW particles reached the size of the mesopores in SBA-15 silica. This can be seen on the micro-

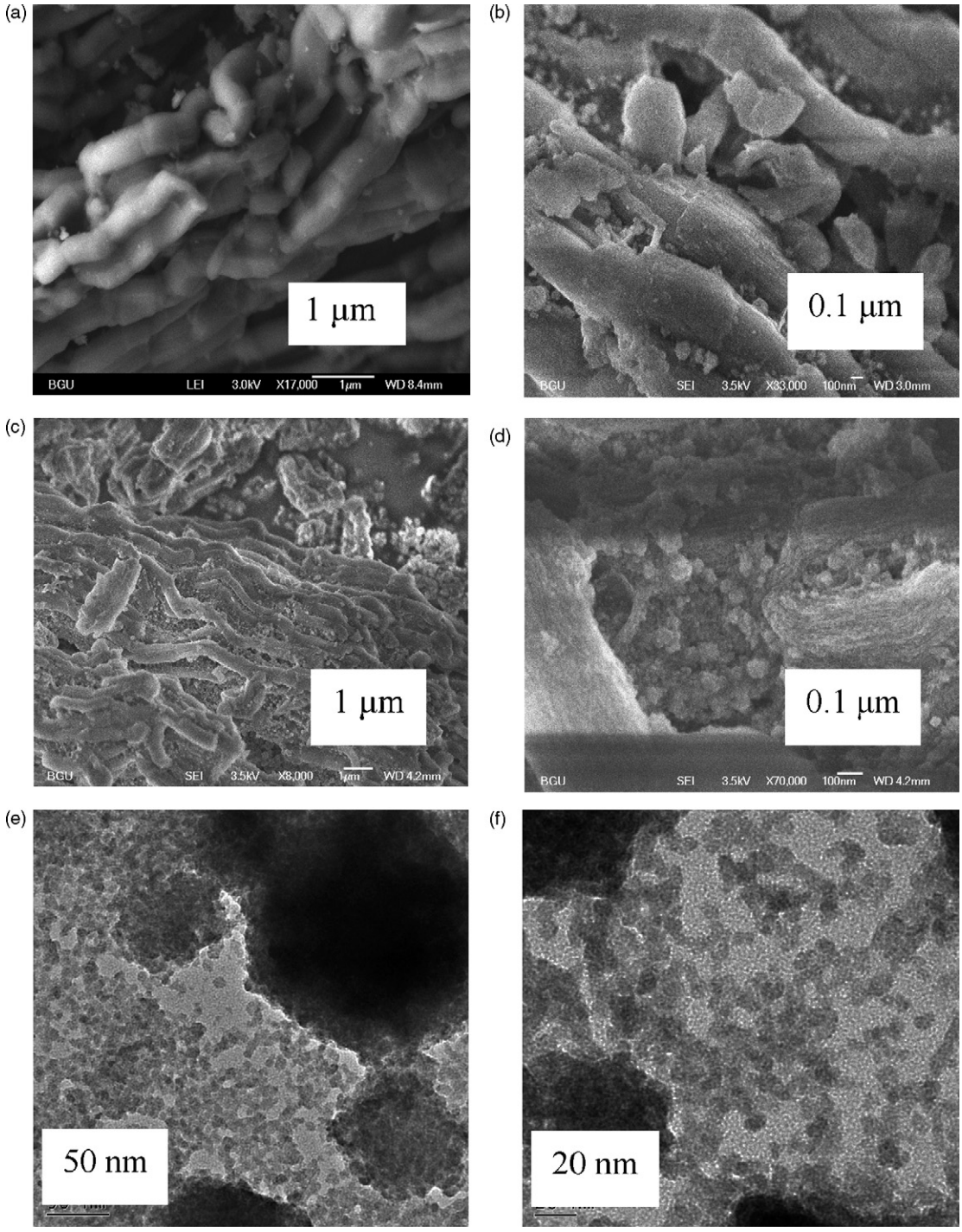

Fig. 1. SEM images of as-prepared CsHPW/SBA-P composite (a), partially desilicated CsHPW/SBA-HF-1P (b) and CsHPW/SBA-HF-3P (c, d), and HRTEM micrographs of CsHPW/SBA-HF-5P (e) and CsHPW/SBA-HF-2A (e) nanocasts.

graphs, where the microtomes were oriented perpendicular to the silica mesopore channels (Fig. 2b and d). These particles can plug the mesopores, blocking the access of molecules to part of the CsHPW nanoparticles. Partial removal of silica by HF liberated the CsHPW nanocrystals. They became visible in the SEM images as 20–50 nm aggregates located between the silica microfibers and their amounts increased proportional to the extent of desilication of the CsHPW/SBA-15 composites (Fig. 1b–d). After removal of more than 95% of the silica the nanocasts, obtained with both Cs-precursors, consisted of large aggregates of primary CsHPW nanocrystals up to 200 nm (Fig. 1e and f). The isolated primary 5–9 nm nanoparticles of CsHPW were also detected at the HRTEM micrographs (Fig. 1e and f). They became visible after partial destruction of the aggregates by ultrasonication, used for sample deposition on the Cu-grid.

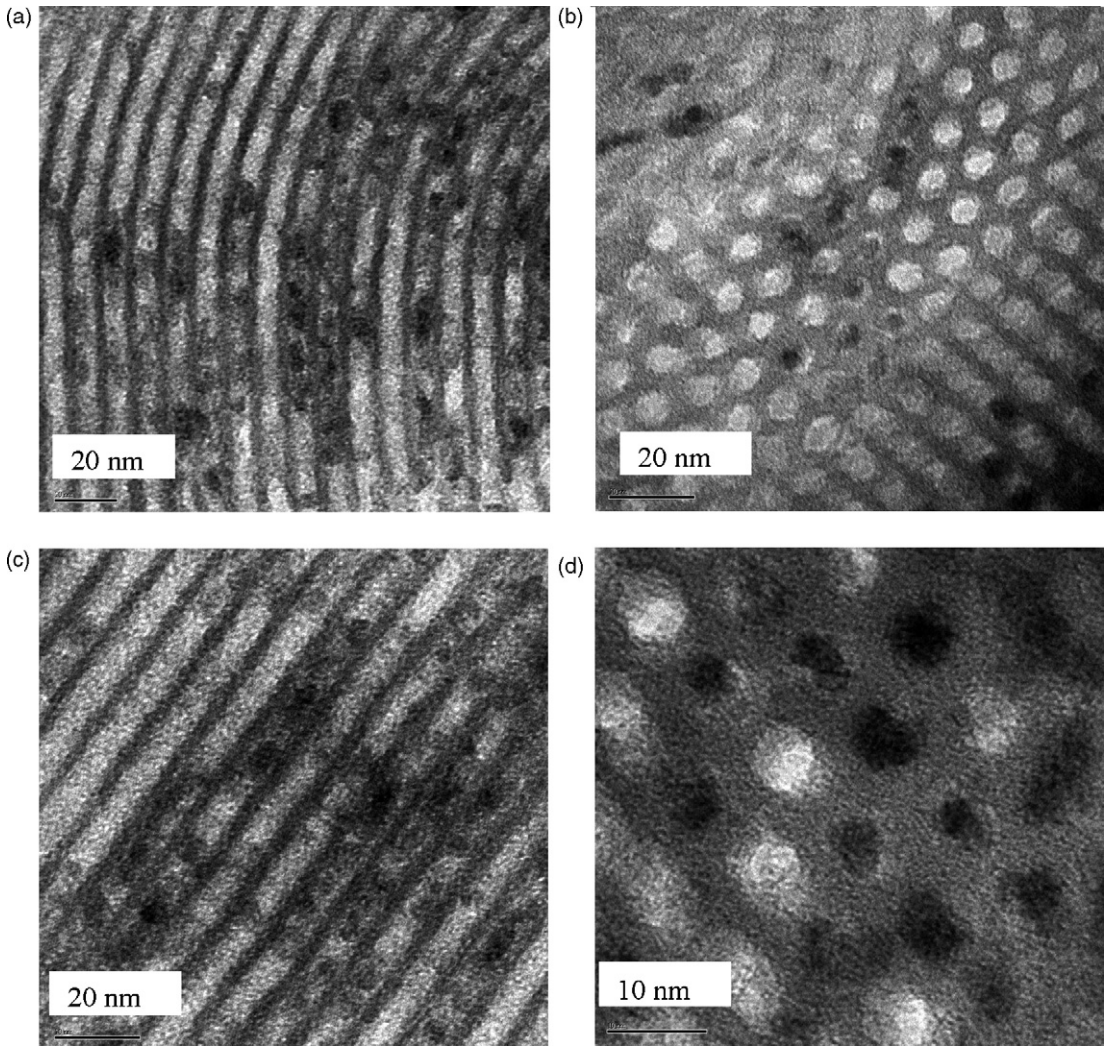

Fig. 2. HRTEM micrographs of as-prepared CsHPW/SBA-P (a, b) and CsHPW-A (c, d) composites recorded at side (a, c) and frontal (b, d) orientations of microtome relative to the SBA-15 microfibers axis.

3.5. XRD analysis

The XRD patterns of the as-prepared CsHPW/SBA-P composite and the CsHPW nanocasts obtained with both Cs-precursors are shown in Fig. 3, together with the X-ray diffractogram of the reference co-precipitated $Cs_{2.5}H_{0.5}PW_{12}O_{40}$ material. The CsHPW phase inside the CsHPW/SBA-15 composites showed the same bcc cubic structure as the reference co-precipitated $Cs_{2.5}H_{0.5}PW_{12}O_{40}$ salt. Broadening of the diffraction peaks of the composites relative to the reference bulk CsHPW material reveals that the crystal domain size of CsHPW phase in composites is twice as low as in the reference material (7–7.5 nm versus 13 nm). This is clearly shown in the inset of Fig. 3 for the (2 2 2) reflection. The wide amorphous halo centered at $2\theta = 23^\circ$ in the spectra of SBA-15 silica in as-prepared composites completely disappeared for nanocasted materials. Thus, the removal of the silica matrix does not affect the crystal structure and the real chemical composition of the embedded CsHPW phase that is enriched with protons relative to the nominal composition of the reference co-precipitated materials. It leads only to a merging of the 7–7.5 nm nanocrystals that were formerly isolated in SBA-15 mesopores to form aggregates of 100–200 nm (Fig. 1e and f).

3.6. The texture of the materials

Information about the texture of the materials, derived from the N_2-adsorption isotherms as shown in Fig. 4, is consistent with observations made by microscopic and XRD methods. The nitrogen sorption isotherm of type IV with a H1-type hysteresis, characteristic for mesoporous materials with cylindrical pores such as SBA-15 (Fig. 4(1)), did not change after deposition the CsHPW phase inside the SBA-15 using both Cs-precursors. However, the introduction of the CsHPW phase by means of the reaction deposition technique caused a significant decrease of the pore volume (lowering of the isotherms ordinates at the same P/P_0 values) and a shift of the position of the hysteresis loop to lower P/P_0 values (Fig. 4(2 and 3)). These changes reflect that part of the mesopore volume in the SBA-15 matrix is filled with CsHPW nanocrystals, resulting in pore diameters that are less or equal to that of silica channels, in full agreement with HRTEM data (Fig. 2). As a consequence, the pore size distri-

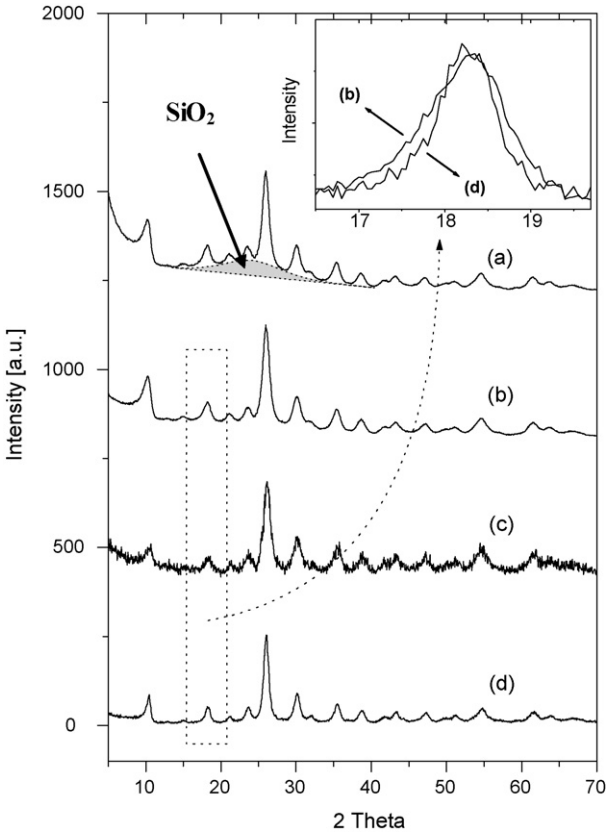

Fig. 3. XRD patterns of as-prepared CsHPW/SBA-P material (a), the same material after removal of silica matrix CsHPW/SBA-HF-5P (b), nanocasted CsHPW/SBA-HF-2A (c) and reference bulk $Cs_{2.5}H_{0.5}PW_{12}O_{40}$ (d).

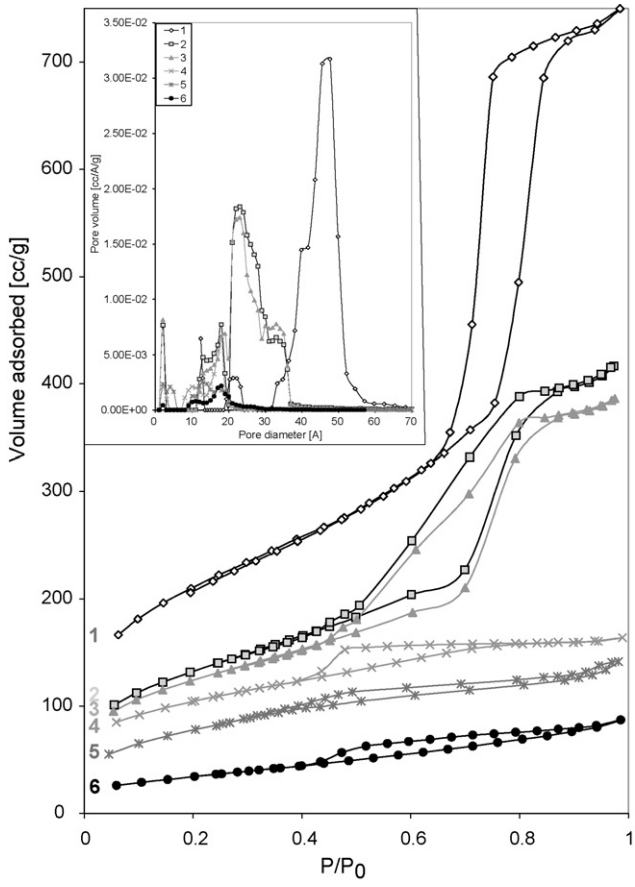

Fig. 4. N_2-adsorption–desorption isotherms recorded with parent SBA-15 (1), CsHPW-loaded CsHPW/SBA-A (2), CsHPW/SBA-P (3), their nanocasts CsHPW/SBA-HF-2A (5), CsHPW/SBA-HF-5P (6) and reference bulk $Cs_{2.5}H_{0.5}PW_{12}O_{40}$ (4); materials (denomination according to Table 1). Ther pore size distributions derived from isotherms (1) to (6) are shown in inset.

butions of CsHPW/SBA-15 composites were shifted to smaller pore diameters of size 2–4 nm (Fig. 4, inset) reflected also by the lowering of the mean pore diameter calculated as a ratio of the pore volume to surface area (Table 1). This is consistent with the close CsHPW loading, dispersion and distribution of nanocrystals in the silica matrix for both composites. Estimation of the normalized surface areas yielded values of NSA equal to 0.85 for CsHPW/SBA-P and to 0.98 for CsHPW/SBA-A. These values were obtained [28] according to the equality:

$$\mathrm{NSA} = \frac{\mathrm{SA}}{1-y}\mathrm{SA}_{\mathrm{SBA}},$$

where SA and SA_{SBA} are the surface areas of the CsHPW/SBA-15 composites and the parent SBA-15 and y the weight fraction of CsHPW in the composites. Assuming a complete blocking of the micropores in SBA-15, after the initial insertion of cesium and a significant blocking of the mesopores by the large CsHPW nanocrystals, as expected from HRTEM data, these relatively high NSA values should be attributed to the high surface area of the embedded CsHPW phase itself. This conclusion is consistent with the appearance of pore size distributions for the micropores with diameters of <2 nm in the composites (Fig. 4, inset). This should be attributed to the embedded CsHPW nanoparticles and the voids between them and the walls of SBA-15 silica channels.

After the removal of the silica matrix the nitrogen sorption isotherms of the CsHPW nanocasts changed their type to I shape with small slopes of the plateau and H4 hysteresis loop, as shown in Fig. 4(5 and 6). The size of hysteresis loop decreased significantly. This reflects the drastic drop of the mesoporosity of the materials which, according to the new shape of the hysteresis loop, can be attributed to slit-shaped pores formed between the CsHPW nanocrystals in their aggregates detected by HRTEM (Fig. 1e and f). The NLDFT analysis of the isotherm gave a picture of the porous structure of the nanocasted CsHPW materials that can be compared with that of the reference bulk salt $Cs_{2.5}H_{0.5}PW_{12}O_{40}$ (Fig. 4, inset). Both the nanocasts, prepared using different Cs-precursors, as well as the reference CsHPW salt did not contain pores with diameter larger than 2.5 nm. The pore structures of all these materials that did not contain a silica scaffold could be characterized by similar pore distributions at pore diameters less than 2.5 nm. The surface area and pore volume of the materials increased according to CsHPW/SBA-HF-5P < CsHPW/SBA-HF-2A < $Cs_{2.5}H_{0.5}PW_{12}O_{40}$ (Table 1, Fig. 4).

It is well established that in CsHPW salts obtained by co-precipitation – the only strategy used for their preparation until now – the surface area is very low (<2 $m^2\,g^{-1}$) for $Cs/W_{12} \leq 2$ and starts to rise for increasing Cs/W_{12} ratios, reaching ~150 $m^2\,g^{-1}$ at $Cs/W_{12} = 2.5$ [6,28]. The CsHPW

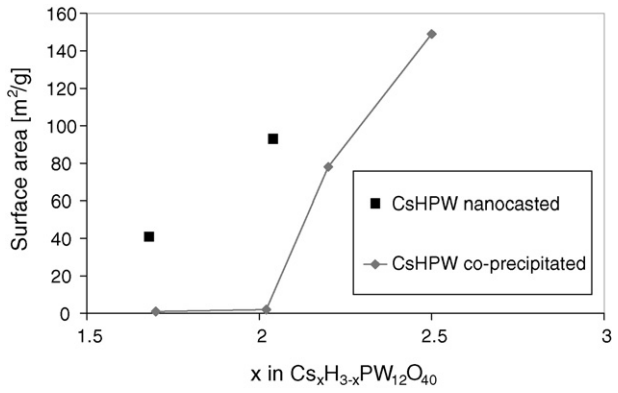

Fig. 5. Surface area of materials prepared by co-precipitation (titration) and nanocasting methods as a function of $Cs^+ \leftrightarrow H^+$ replacement extent.

materials obtained in the present work by the nanocasting strategy demonstrated textural properties characteristic for co-precipitated CsHPW salts with $Cs/W_{12} > 2$ at substantially lower Cs/W_{12} ratios between 1.7 and 2.0. This is clearly demonstrated in Fig. 5 where surface areas measured for bulk CsHPW salts synthesized by co-precipitation at $Cs/W_{12} = 1.7$, 2.0, 2.2 and 2.5, are compared with surface areas of nanocasted CsHPW materials prepared with both Cs-precursors. At the same Cs/W_{12} ratios the nanocasted materials demonstrated surface areas greater by a factor of 41–45 relative to their co-precipitated analogs. The nitrogen sorption isotherms recorded from co-precipitated CsHPW salts at $Cs/W_{12} = 1.7$ and 2.0 were of type II, characteristic for non-porous particles. In contrast, as already mentioned above, the nitrogen sorption isotherms recorded from nanocasted CsHPW materials were of the type I with small slops of the plateu and hysteresis loops, characteristic for microporous materials with significant mesoporosity. Replacing the Cs-carbonate for Cs-acetate or Cs-propoxide in preparation of CsHPW by co-precipitation according to formerly described procedure did not change significantly the texture characteristics of CsHPW salts. That is, the surface area of the CsHPW material with Cs/W_{12} ratio of 2.0 prepared by co-precipitation using $CsCH_3COO$ salt was 4 $m^2\,g^{-1}$, and it did not contain micropores. This confirms the statement that the high surface area of CsHPW nanocasts at $Cs/W_{12} \leq 2$ is caused exclusively by their preparation strategy.

In summary, the implementation of our nanocasting strategy for the preparation of CsHPW salts shifts the Cs/W_{12} ratio where the materials demonstrate high surface areas, significantly to the left, *i.e.* to the range of lower Cs/W_{12} values. This could be rationalized based on the widely accepted mechanism of formation of porous structures in co-precipitated CsHPW materials [2,6,29–31]. During co-precipitation $Cs_3PW_{12}O_{40}$ crystallites with sizes of 10–13 nm are formed at first and then become epitaxially covered by $H_3PW_{12}O_{40}$. A stoichiometry of $Cs/W_{12} = 2$ corresponds to a full coverage of these $Cs_3PW_{12}O_{40}$ cubic crystals. They aggregate into non-porous dense polycrystalline materials with particle sizes of about 1000 nm and with negligible porosity and a surface area, where the inter-sites between the primary nanocrystals are filled with $H_3PW_{12}O_{40}$ material [6]. At higher Cs/W_{12} ratios the CsHPW material became a solid solution of $Cs_3PW_{12}O_{40}$ with a substantially lower relative amount of $H_3PW_{12}O_{40}$, leaving void spaces between the primary nanocrystals. The latter being only loosely aggregated demonstrated significant porosity and a high surface area.

The texture of CsHPW materials formed by the nanocasting preparation strategy can be envisioned as shown in Fig. 6. The $H_3PW_{12}O_{40}$ molecules that entered inside the SBA-15 mesopores, but did not reacted with the immobilized Cs-ions, are washed out at the last step of the reaction deposition procedure. It is known that the adsorbed $H_3PW_{12}O_{40}$ is easily removed even from dried HPW/SBA-15 composites by simple washing in water or alcohols [4]. Thus, the primary building blocks for the formation of cubic CsHPW nanocrystals inside the SBA-15 channels of the CsHPW/SBA-15 composites are heteropolyanions with 1–3 Cs^+-ions, according to the scheme presented at Fig. 6a. Due to the replacement of immobilized Cs^+-ions by protons of heteropolyacid molecules, the latter are converted into mobile molecules with partially or fully exchanged Cs of low solubility that crystallize inside the silica mesopores. We can thus propose that after calcination at 573 K, favoring migration of H^+ and Cs^+ ions [6], the primary nanocrystals are solid solutions with random distributions of cations in the bulk that do not contain adsorbed $H_3PW_{12}O_{40}$ species at their external surface. These primary nanocrystals, after removal of the SBA-15 scaffold following the scheme presented at Fig. 6b, become loosely aggregated in the form of secondary particles of size 50–200 nm (HRTEM) with significant porosity and high surface area.

Calculation of the particle sizes of both nanocasts from their surface area, according to the equality:

$$d = \frac{6000}{\rho \times \mathrm{SA}},$$

where ρ is the density (in g cm^{-3}), estimated from the average lattice constant and the molecular weight of salts with $Cs/W_{12} = 1$–3, and SA the surface area (in $m^2\,g^{-1}$), gave values of 23 and 10 nm for CsHPW/SBA-HF-5P and CsHPW/SBA-HF-2A, respectively. These values are not far from the real d values derived from XRD and HRTEM data and are evident for partial blockage of the surface of the primary nanocrystals in the aggregates—more in the CsHPW/SBA-HF-5P nanocast.

The lower surface area, 41 $m^2\,g^{-1}$, of the CsHPW nanocast with a Cs/W_{12} ratio of 1.7 compared with the area (93 $m^2\,g^{-1}$) of the nanocast having a Cs/W_{12} ratio of 2.0 can be attributed to the higher extent of hydration for material with elevated protons concentration thus favoring the more dense packing of the primary crystals in the CsHPW/SBA-HF-5P nanocast decreasing the porosity (Table 1). Another reason for it can be a partial conversion of the CsHPW phase with some random cation distribution to the thermodynamically more stable $Cs_3PW_{12}O_{40}$. The covering with $H_3PW_{12}O_{40}$ moieties liberating in higher amount in case of CsHPW/SBA-HF-5P material would block part of the micro- and mesopores in the structure of these proton-enriched materials.

The both explanations are consistent with observations that the HPW material does not contain micropores while the micropore surface area linearly increases from 19 to 68 and then to 119 $m^2\,g^{-1}$ (t-plot estimation) by passing from CsHPW/SBA-HF-5P to CsHPW/SBA-HF-2A and then to the

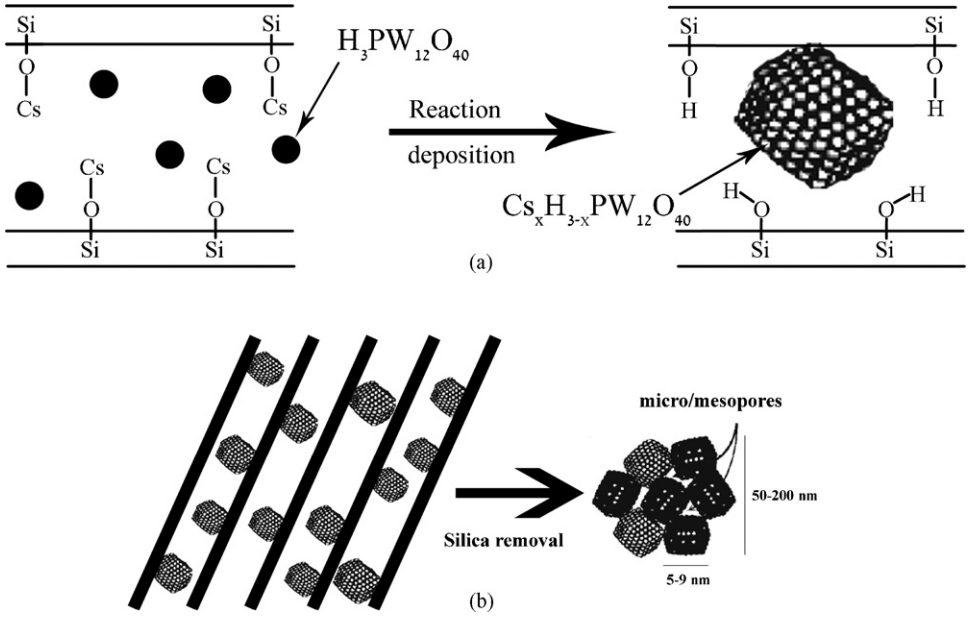

Fig. 6. Proposed model for formation of microstructures of nanocasted CsHPW material.

bulk $Cs_{2.5}H_{0.5}PW_{12}O_{40}$ materials, respectively, with increasing the $x = Cs/W_{12}$ value from 1.7 to 2.5. In the range of $x \leq 2$ the surface areas of co-precipitated materials are significantly lower (Fig. 5) due full blocking of micropores with $H_3PW_{12}O_{40}$ moieties for co-precipitated materials.

3.7. Local structure of the polyanions by NMR

Information about the molecular composition of the CsHPW nanocasts was obtained by using solid state NMR. Multi-spin MAS NMR spectra were collected from a set of samples that represent the preparation procedure of these nanocasts. In particular spectra from Cs/SBA-P and Cs/SBA-A, CsHPW/SBA-P and CsHPW/SBA-A as well as CsHPW/SBA-HF-5P and CsHPW/SBA-HF-2A were recorded and compared.

3.7.1. ^{31}P NMR results

The sensitivity of the chemical shift value of the phosphorous atom at the center of the HPW Keggin units has been used to follow their acidic environment [32,33]. Variations of this value, between −16 and −11 ppm, were correlated to changes in the average charge compensation of the $(PW_{12}O_{40})^{3-}$ anions characterized by $H^+ - kH_2O$ with k between 2 and 0 [33–35].

In a HPW sample composed of large crystals the majority of the Keggin units are coordinated to their neighboring units by H_3O^+ and result in a ^{31}P line with a chemical shift around −15.5 ppm. An example of a ^{31}P spectrum of a bulk HPW sample with crystals of size ∼85 nm, as determined from XRD data, is shown in Fig. 7a. This spectrum was presented earlier [4] and can be decomposed in terms of a major line (65%) at −15.5 ppm, due to Keggin units inside the crystals, and two additional lines at −16 and −16.5 ppm, presumably caused by Keggin units experiencing surface effects or crystal imperfections. $Cs_{2.5}H_{0.5}PW_{12}O_{40}$ crystals of 13 nm, obtained after a co-precipitation of Cs_2CO_3 and HPW in aqueous solution, resulted in a single narrow ^{31}P line at −14.6 ppm (not shown).

The ^{31}P line of the CsHPW/SBA-P sample was positioned at −14.8 ppm and of CsHPW/SBA-A at −14.1 ppm (Fig. 7A(b) and (c)). Removal of the silica matrix resulted for both samples in a line (Fig. 7A(d) and (e)) at about −14.8 ppm. Deconvolution in terms of Lorenzian lineshapes of these lines showed some fine structure, however the differences in positions (±0.15 ppm) of the individual components are much smaller than their linewidths (∼0.6 ppm). We therefore preferred not to draw any conclusion from these components. The increase in the electron density after a gradual exchange of protons by Cs^+ ions in hydrated Keggin anions has been shown to cause a shift of the ^{31}P peak to lower field, *e.g.* a shift of about 0.5 ppm was recorded for Cs/W_{12} values reaching 2.5 [36,37]. Thus the appearance of higher field peaks centered around −14.8 ppm in the ^{31}P NMR spectra of the nanocasted samples, relative to −14.6 ppm for the bulk reference $Cs_{2.5}H_{0.5}PW_{12}O_{40}$ material, must reflect the lowering of the Cs/W_{12} values in parts of the nanocasts. The appearance of the −14.1 peak in the spectra of CsHPW/SBA-2A is an indication of a relative high concentration of Cs^+ in this material. The overall similarity of the chemical shift values in both the CsHPW/SBA composites and their corresponding nanocasts is an additional indication that the HF treatment did not influence the structure of the Keggin units significantly.

3.7.2. ^{133}Cs NMR results

NMR spectra of ^{133}Cs absorbed on SBA-15, on HPW crystals inside SBA-15 and in the final catalysts were also recorded. Adsorption of cesium on SBA-15 resulted in a broad (15–20 ppm) spectral line at −21 ppm for Cs/SBA-A and −5 ppm for Cs/SBA-P (Fig. 7B(a) and (b)). Deconvolution of these lines with Lorenzian line did not provide any insight about the nature of the shape of the lines and their broadening. No spinning side bands were observed, indicating some isotropic

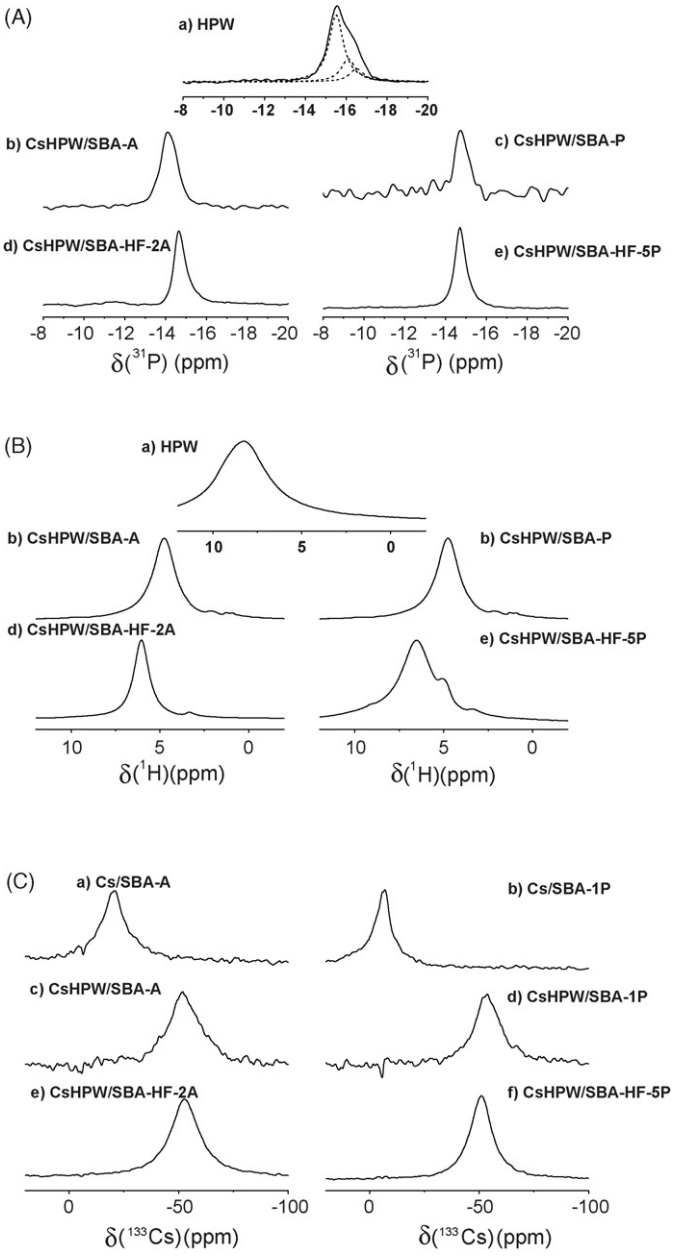

Fig. 7. ^{31}P (A), ^{133}Cs (B) and ^{1}H (C) MAS NMR spectra recorded with CsHPW-loaded SBA-15 materials and their nanocasts (samples denomination according to Table 1).

environment of the cesium nuclei due to motion or non-specific binding. Chemical shift values of ^{133}Cs are known to be very sensitive to their chemical coordination and surrounding humidity [36,37]. The values measured in our samples suggest that the cesium atoms belong to the inner-sphere complexes, *i.e.* are directly coordinated to the inner surface of the SBA-15 channels [37]. The difference between the chemical shift values of the two samples of ∼16 ppm can be indicative for a difference in the surface coordination or local water content of the two samples [37]. This is then the result of the location of higher portions of Cs^+ ions inside the micropores of SBA-15 silica in Cs/SBA-P relative to Cs/SBA-A, as was concluded before.

After the addition of the HPW to the sample Cs/SBA-A the ^{133}Cs line shifted to −54 ppm and showed some sidebands with relative intensities of about 14%. The CsHPW/SBA-P sample gave a similar result at −53 ppm and a sideband intensity of about 20%. The centre band regions of these spectra are shown in Fig. 7B(c) and (d). The appearance of sidebands suggests that the cesium atoms are chemically bound to HPW. The lineshapes of these sidebands differ from the shape of the centre band, which indicates that some molecular distribution exists in the sample. We can thus conclude that part of the HPW molecules reacted with the immobilized cesium ions during step (2) of the reaction deposition, resulting in a partially coating of HPW by cesium.

The removal of the SBA matrix leaves the line at about the same positions: −53 ppm for CsHPW/SBA-HF-2A and −51 ppm for CsHPW/SBA-HF-5P (Fig. 7B(e) and (f)). The overall crystalline and coating characteristics of the CsHPW material were thus not modified during the HF treatment, leaving the cesium to HPW crystal binding in tact in the CsHPW nanocasts. For comparison a sample of CsHPW, prepared without using a SBA-15 intermediate, resulted in spectra consisting of a main line at −54 ppm (80% with 12% sideband intensity), an additional line at −41 ppm (9% with 2.5% sideband intensity) and a small sharp line at −46.4 ppm without sidebands (not shown).

3.7.3. ^{1}H NMR results

To identify the acid character of the Cs-coated HPW crystallites some ^{1}H NMR experiments were also performed on the samples. Bulk HPW with large crystallite sizes exhibited after drying a broad proton line at about 7.5 ppm (Fig. 7C(a)). This line must be attributed to the hydroxonium H_3O^+ protons inside the HPW crystals. Addition of the HPW to the cesium loaded SBA-15 samples resulted in spectra showing a significant amounts of water, with a line at about 4.9 ppm, in these samples. Even after calcination at 573 K the residual ^{1}H line with a width of 3 ppm had a shift value of 4.8 ppm (Fig. 7C(b) and(c)). This is perhaps not surprising realizing again that only 15% of the inner surface of the SBA-15 is covered with Cs_xH_{3-x}HPW crystals and their proton signal is embedded in the baseline of the broad water peak. Some hydroxyl resonances at 1–2 ppm are also present in the sample.

After the SBA-15 removal and a drying procedure the ^{1}H spectra (Fig. 7C(d) and (e)) show their main lines at 6.3 and 6.5 ppm for CsHPW/SBA-HF-2A and CsHPW/SBA-HF-5P, respectively. In the last spectrum the line is relatively broad and an additional line at 4.9 ppm is clearly observed. Some residual free water, resonating at about 4.9 ppm, can be trapped in these samples. In small size crystallites the hydroxonium protons exchange between each other and surface protons, apparently resulting in the lines at about 6.4 ppm. The difference between this 6.4 and the 7.5 ppm line of bulk HPW is then a consequence of the decrease in size of the crystallites (from ∼85 to ∼7 nm).

From all the NMR results we can thus conclude that the final Cs_xH_{3-x}HPW nanocasts are composed of partially cesium exchanged HPW molecules, created and crystallized inside the SBA-15 that maintained their structure after the removal of SBA-15 matrix by the HF treatment. The NMR information about the

Table 2
Estimation of relative surface acidity in co-precipitated and nanocasted CsHPW materials

Material	(3–x)	d (nm)	Number of Keggin units per crystal edge	Total number of Keggin units per crystal	Number of surface Keggin units per crystal	(%) Keggin units exposed	Surface area (m^2/g)	[H^+/g] rel. (a.u.)
Bulk CsHPW	0.5	13	11	1331	602	45	149	1
CsHPW/SBA-HF-2A	1.0	7	6	216	144	67	93	1.9
CsHPW/SBA-HF-5P	1.3	7.5	6	216	144	67	43	1.2

local structure of the polyanions is therefore consistent with the chemical composition and alteration of the structure–texture characteristics of the materials at the different preparation steps as presented in Fig. 6.

3.8. Surface acidity and catalytic performance

The proton enrichment of the CsHPW nanocasts relative to the reference co-precipitated material, manifested by higher (3–x) values in formula $Cs_xH_{(3-x)}PW_{12}O_{40}$, can yield increased surface acidity and catalytic activity. The condition for this is a favorable combination of the value (3–x) characterizing the total proton content, the percentage of exposure of Keggin units (E) at the surface of the primary crystals and the total surface area (SA) of the materials, characterizing the availability of this surface in the crystal aggregates. The exposure of Keggin units can be estimated based on the model assuming that the primary crystals of CsHPW are cubic crystals that are built of densely packed nearly spherical Keggin units with a lattice constant of about 1.2 nm and crystal size 7–13 nm both estimated from the XRD patterns of materials [6a]. The crystal sizes, the total amounts of Keggin units as well as the number of Keggin units located at the external crystal planes enable the calculation of the percentage of exposed Keggin units, as shown in Table 2. The number of protons per gram [H^+/g] available for reaction with molecules at the external surface of the CsHPW crystals in a material can be expressed as a product of the above mentioned values multiplied by their corresponding proportionality k-coefficients, according to:

$$[H^+/g] = k_1(3 - x)k_2Ek_3\,SA$$

The exact values of these coefficients k_1, k_2 and k_3 are not known. They depend on the density of the material, the character of the protons exposure at the surface Keggin units, the aggregation mode of the primary crystals and more. The crystal structure of all studied CsHPW materials and the valence states of the Cs, P, W and O atoms, based on the XRD, MAS NMR, HRTEM, HRSEM and XPS characterization methods used in reference [16] and in the present work, are similar. Therefore it is reasonable to assume that the coefficients k_1, k_2 and k_3 will have the same values for our nanocasts and for the co-precipitated CsHPW material. If so the relative proton concentrations can be calculated from the data presented in Table 2 as following:

$$[H^+/g]_{rel.} = I_{CsHPW}/I_{ref.CsHPW} \quad (3)$$

where I is equal to the product (3–x)E × SA. The accuracy of such calculation would be reasonable for future comparison with the measured acidity and performance in acid catalyzed reactions. The estimation showed (Table 2) that the surface acidity of nanocasts should be higher compared with that of co-precipitated $Cs_{2.5}H_{0.5}PW_{12}O_{40}$ material by a factor of 1.2–1.9.

3.8.1. NH_3-TPD results

The NH_3-TPD spectra of the reference co-precipitated material $Cs_{2.5}H_{0.5}PW_{12}O_{40}$ and of both nanocasts are shown in Fig. 8. The wide NH_3-desorption peaks recorded with nanocasted CsHPW materials in the temperature range 450–950 K were close to that observed for heteropolyacid stabilized in silica matrix [16,38]. The integrated intensities of the spectra in this temperature range where the sample structures are retained according to XRD can be considered as proportional to the concentration (NH_3 g^{-1}) of available protons, and thus the materials acidity. A comparison between these intensities shows that the values of the relative acidities (in parentheses) of the materials follow the trend:

$$Cs_{2.5}H_{0.5}PW_{12}O_{40}(1) < CsHPW/SBA\text{-}HF\text{-}5P(1.8) < CsHPW/SBA\text{-}HF\text{-}2A(2.7).$$

This same trend can be deduced from model estimations. The measured relative acidities for the nanocasts (1.8; 2.7) were higher by about 50% compared with their estimated values obtained from Eq. (3) (1.2; 1.9, Table 2). The reason for this improvement may be a better exposure of protons at the surface of primary CsHPW crystals in the nanocasts than in co-precipitated materials. The value of (3–x)/2 for the amount of exposed protons per surface Keggin unit that gave a good

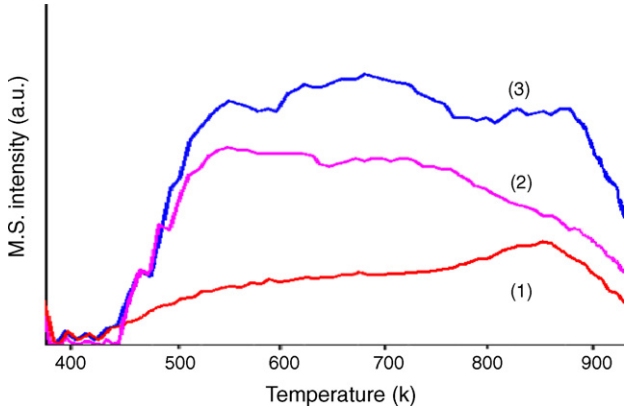

Fig. 8. Ammonia TPD patterns of the reference bulk co-precipitateed $Cs_{2.5}H_{0.5}PW_{12}O_{40}$ (1), nanocasted CsHPW/SBA-HF-5P (2) and CsHPW/SBA-HF-2A (3) materials.

Table 3
Catalytic performance of CsHPW/SBA composites, 'nanocasted' and bulk CsHPW materials measured in acid-catalyzed reactions

Catalyst	Reaction rate ($mmol\,h^{-1}\,g\,cat^{-1}/\times 10^3\,mmol\,h^{-1}\,m^{-2}$)	
	MTBE synthesis	*Iso*-propanol dehydration
CsHPW/SBA-P	88	293
CsHPW/SBA-HF-1P	110	–
CsHPW/SBA-HF-2P	209	–
CsHPW/SBA-HF-3P	352	907
CsHPW/SBA-HF-4P	375	–
CsHPW/SBA-HF-5P	447/(218)	1400/(683)
CsHPW/SBA-A	147	347
CsHPW/SBA-HF-1A	470	1320
CsHPW/SBA-HF-2A	643/(138)	1667/(358)
Bulk CsHPW	195/(28)	613/(88)

correlation between the calculated and measured acidity of co-precipitated CsHPW materials [20,39], must be higher in nanocasts. This can be a result of the difference in the formation mechanisms of the primary CsHPW crystals, *i.e.* the aggregation of partially Cs-exchanged Keggin units inside the SBA-15 channels during the preparation of the nanocasts precursor versus the penetration of adsorbed $H_3PW_{12}O_{40}$ molecules inside the primary $Cs_3PW_{12}O_{40}$ crystals during the synthesis of the co-precipitated material.

3.8.2. Testing the catalytic performance

The performance of the CsHPW/SBA-15 composites with different extents of desilication and of the reference co-precipitated $Cs_{2.5}H_{0.5}PW_{12}O_{40}$ material in selected acid catalyzed reactions is shown in Table 3. An increase of the weight fraction of the active phase in both CsHPW/SBA composites caused an increase of the substrates conversion rates measured in both tested reactions on the catalysts weight basis. Important that increasing the content of the active CsHPW phase with gradual removal of silica caused the increase of reactions rates by a factor of about 5 (Table 3)—much more than it was expected from the increasing of its weight fraction in catalytic materials by a factor of 2.1–2.3 (Table 1). This is a result of increasing the accessibility of active CsHPW phase after liberation from SBA-15 matrix. It yields a rise of the visible reaction rate in addition to that observed as a result of increasing the loading of active CsHPW phase. This effect is consistent with partial blocking of CsHPW nanoparticles inside the SBA-15 channels observed before (HRTEM, normalized surface area).

The activity of nanocasts containing less than 5 wt.% residual silica surpassed that of the reference co-precipitated bulk salt in both reactions. The highest activity per gram of catalyst was measured with the CsHPW/SBA-HF-2A material. It exceeded the activity of the reference co-precipitated $Cs_{2.5}H_{0.5}PW_{12}O_{40}$ salt by a factor of 3.3 for MTBE synthesis and 2.7 for *iso*-propanol dehydration. Plotting the relative values of the reactions rates normalized per gram of CsHPW phase, $A_{CsHPW}/A_{ref.CsHPW}$, as well as the estimated (Table 2) and measured (Fig. 8) relative acidities versus the values of (3–x) in

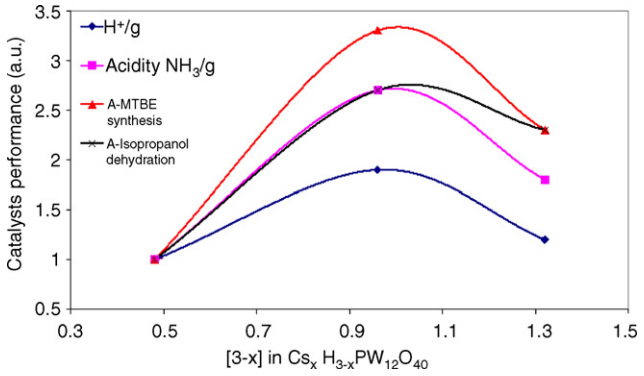

Fig. 9. Correlations of catalytic activity and surface acidity for co-precipitated and nanocasted CsHPW materials.

the composition of Cs_xH_{3-x} $PW_{12}O_{40}$ materials demonstrates a good acidity-to-activity correlation (Fig. 9). This confirms the validity of the used model assuming NH_3 adsorption into the bulk or at the surface of CsHPW nanocrystals and equal reactions turnovers at the acid sites in all the three CsHPW materials. It shows full agreement between the proposed model and the specific activities measured in terms of the reaction rates normalized per 1 m^2 of catalytic materials (Table 3). The figures of specific activities show a maximum for the CsHPW/SBA-HF-5P nanocast with the highest protons concentration [(3–x) = 1.3]. The lower surface area of this material (Table 1) renders this nanocast less active on the weight basis compared with CsHPW/SBA-HF-2A.

4. Conclusions

Preparation of CsHPW salts, supported on mesostructured SBA-15 silica, by the reaction deposition strategy causes the formation of isolated CsHPW nanocrystals inside the nanotubular channels of SBA-15 that have Cs/W_{12} ratios significantly lower than in their nominal composition. This is a result of the fixation of part of the Cs^+ cations inside the micropores causing them to be non available for reaction with $H_3PW_{12}O_{40}$ molecules. The surface area of the proton-enriched nanocrystalline aggregates formed after desilication of the CsHPW/SBA composites is by a factor of about 40 higher than that of the co-precipitated CsHPW salts with the same composition. This yields a material with a surface acidity that is higher by a factor of about 2–3 than that of the co-precipitated $Cs_{2.5}H_{0.5}PW_{12}O_{40}$ salt. The catalytic activity of this nanocasted CsHPW material exceeds that of the $Cs_{2.5}H_{0.5}PW_{12}O_{40}$ that has been known as the most active among the acidic CsHPW salts, by a factor of 2–3.

Acknowledgements

This study was supported by the Israeli Science Foundation (Grants nos. 8003 and 739/06). The authors gratefully acknowledge Dr. V. Esersky for HRTEM, Mrs. L. Burlaka for HRSEM and Dr. A. Erenburg for conducting the XRD characterizations.

References

[1] M. Guisnet, Ph. Bichon, N.S. Gnep, N. Essayem, Top. Catal. 11/12 (2000) 247–254.
[2] M. Misono, Chem. Commun. (2001) 1141–1152.
[3] J. Kaur, K. Griffin, B. Harrison, I.V. Kozhevnikov, J. Catal. 208 (2002) 448–455.
[4] P.M. Rao, A. Wolfson, S. Kababya, S. Vega, M.V. Landau, J. Catal. 232 (2005) 210–225.
[5] S. Tatematsu, T. Hibi, T. Okuhara, M. Misono, Chem. Lett. (1984) 865–868.
[6] (a) T. Okuhara, H. Watanabe, H.T. Nishimura, K. Inumaru, M. Misono, Chem. Mater. 12 (2000) 2230–2238;
(b) M. Yoshimune, Y. Yoshinada, T. Okuhara, Micropor. Mesopor. Mater. 51 (2002) 165–174.
[7] (a) J.B. McMonagle, J.B. Moffat, J. Colloid. Interface Sci. 101 (1984) 479–488;
(b) J.B. Moffat, J.B. McMonagle, D. Tailor, Solid State Ionics 26 (1988) 101–108.
[8] (a) T. Okuhara, N. Mizuno, M. Misono, Appl. Catal. A 222 (2001) 63–77;
(b) T. Okuhara, Appl. Catal. A 256 (2003) 213–224.
[9] T. Okuhara, M. Kimura, T. Kawai, Z. Xu, T. Nakato, Catal. Today 45 (1998) 73–77.
[10] S. Soled, S. Miseo, G. McVicker, W.E. Gates, A. Gutierrez, J. Paes, Catal. Today 36 (1997) 441–450.
[11] A. Molnar, T. Beregszaszi, A. Fudala, P. Lentz, J.B. Nagy, Z. Konya, I. Kiricsi, J. Catal. 202 (2001) 379–386.
[12] W. Yang, J. Billy, Y. Ben Taarit, J.C. Vedrine, N. Essayem, Catal. Today 73 (2002) 153–165.
[13] S. Choi, Y. Wang, Z. Nie, J. Liu, C.H.F. Peden, Catal. Today 55 (2000) 117–124.
[14] Y. Wang, C.H.F. Peden, S. Choi, Catal. Lett. 75 (2001) 169–173.
[15] K. Nowinska, W. Kaleta, Appl. Catal. A 203 (2000) 91–100.
[16] P.M. Rao, M.V. Landau, A. Wolfson, A.M. Shapira-Tchelet, M. Herskowitz, Micropor. Mesopor. Mater. 80 (2005) 43–55.
[17] N. Horita, M. Yoshimune, Y. Kamiya, T. Okuhara, Chem. Lett. 34 (2005) 1376–1377.
[18] C.D. Yadav, N.S. Asthana, Appl. Catal. A 244 (2003) 341–357.
[19] F. Zhang, C. Yuan, J. Wang, Y. Kong, H. Zhu, C. Wang, J. Mol. Catal. A 247 (2006) 130–137.
[20] J.A. Dias, E. Caliman, S.C.L. Dias, Micropor. Mesopor. Mater. 76 (2004) 221–232.
[21] M.V. Landau, L. Vradman, V. Valtchev, J. Lezervant, E. Liubich, M. Talianker, Ind. Eng. Chem. Res. 42 (2003) 2773–2782.
[22] T. Valdes-Solis, A.B. Fuertes, Mater. Res. Bull. 41 (2006) 2187–2197.
[23] T. Okuhara, T. Nishimura, H. Watanabe, M. Misono, J. Mol. Catal. A 74 (1992) 247–256.
[24] L. Vradman, M.V. Landau, M. Herskowitz, V. Ezersky, M. Talianker, S. Nikitenko, Y. Koltypin, A. Gedanken, J. Catal. 213 (2003) 163–175.
[25] A. Jarczewski, Can. J. Chem. 64 (1986) 1021–1028.
[26] V. Ramani, H.R. Kunz, J.M. Fenton, Electrochim. Acta 50 (2005) 1181–1187.
[27] G.B. NcGaevey, J.B. Moffat, J. Catal. 130 (1991) 483–497.
[28] L. Vradman, M.V. Landau, D. Kantorovich, Y. Koltypin, A. Gedanken, Micropor. Mesopor. Mater. 79 (2005) 307–318.
[29] T. Okuhara, T. Nishimura, M. Misono, Chem. Lett. (1995) 155–156.
[30] T. Okuhara, T. Nakato, Catal. Surv. Jpn. 2 (1998) 31–44.
[31] N. Nizuno, M. Misono, Chem. Rev. 98 (1998) 199–217.
[32] S. Uchida, K. Inumaru, M. Mosono, J. Phys. Chem. B 104 (2000) 8108.
[33] N. Essayem, Y.Y. Tong, H. Jobic, J.C. Verdine, Appl. Catal. A 194–195 (2000) 109–122.
[34] J.C. Edwards, C.Y. Thiel, B. Benac, J.F. Knifton, Catal. Lett. 51 (1998) 77–83.
[35] M.E. Chimienti, L.R. Pizzio, C.V. Caseres, M.N. Blanco, Appl. Catal. A 208 (2001) 7–19.
[36] Y. Kim, R.J. Kirkpatrick, R.T. Cygan, Geochim. Cosmochim. Acta 60 (1996) 4059–4074.
[37] Y. Kim, R.J. Kirkpatrick, Geochim. Cosmochim. Acta 61 (1997) 5199–5208.
[38] A. Molnar, C. Keresszegi, B. Tőrők, Appl. Catal. A 189 (1999) 217–224.
[39] T. Okuhara, T. Nishimura, M. Misono, in: J.W. Hightover, W.N. Belgass, E. Iglesia, A.T. Bell (Eds.), Proceedings of the 11th International Congress on Catalysis, Elsevier, Amsterdam, 1996, p. 581.